Journal of Particle Science and Technology 9 (2) (2023) 73-84

Iranian Research Organization for Science and Technology (IROST)

Journal of PARTICLE Science & Technology

JPSIT
https://jpst.irost.ir

Online ISSN: 2423-4079
Print ISSN: 2423-4087

Numerical investigation of the effect of nanoparticle sedimentation on the thermal behavior of cavities with different cross-sectional shapes

Miralam Mahdi✉, **Amir Noori, Atie Farrokh**

Faculty of Mechanical Engineering, Shahid Rajaee Teacher Training University, Tehran, Iran

HIGHLIGHTS

- The nanoparticle sedimentation has a significant effect on the thermal behavior of the nanofluid.
- The cross-section geometry of the enclosure and the Rayleigh number are two significant parameters that influence the settling time and the Nusselt number.
- The square cavity has the highest Nusselt number, and this value could be improved by increasing the Rayleigh number.
- The triangular and square cross sections have the shortest and longest sedimentation over time, respectively.

GRAPHICAL ABSTRACT

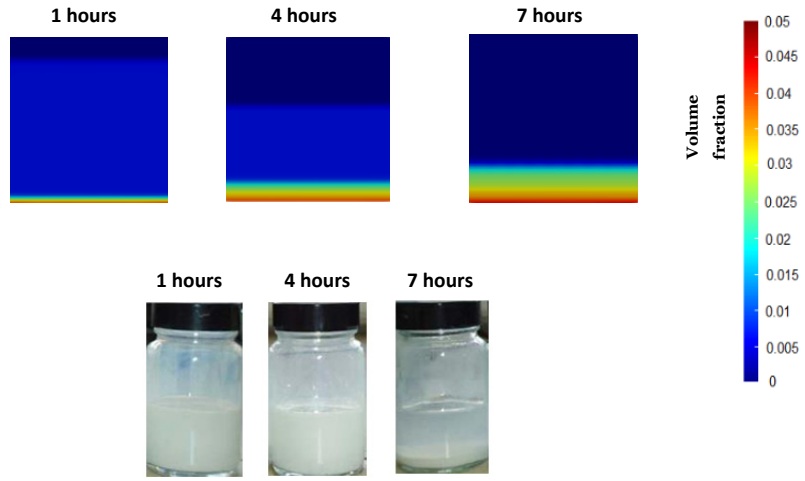

ARTICLE INFO

Article type:

Research article

Article history:

Received 6 November 2023
Received in revised form 1 January 2024
Accepted 2 January 2024

Keywords:

Transient flow
Free convection
Nanoparticles sedimentation
OpenFOAM
Cross-section

DOI: 10.22104/JPST.2024.6586.1245

ABSTRACT

In this paper, the thermal behavior of nanofluids was numerically simulated during nanoparticle sedimentation. Using the finite volume method by combining appropriate solvers, a new solver was developed in the open-source framework, i.e., open Foam. Free convection flow was transiently modeled using this solver during the sedimentation of the second phase (nanoparticles). A relative velocity term from the Vesilind relation was added to the momentum equation to model the sedimentation. Bossiness and Maiga's relations were used to calculate the density changes with temperature and effective conductivity, respectively. Simulations were performed for square, triangular, and circular cross-sections with the same hydraulic diameter at three Rayleigh numbers. In addition, the changes in Nusselt number over time and the distribution of nanoparticles under different conditions were studied. The results showed that forming the sediment layers at the bottom of the enclosure reduced the streamlines and decreased natural convection and rotational flow. In addition, it contributed to conductive heat transfer, leading to a rapid decrease in the Nusselt number of cavities. Moreover, by increasing the Rayleigh number, the square and triangular cross sections had the highest and lowest heat transfer, respectively.

✉ *Corresponding author: E-mail address:* m.mahdi@sru.ac.ir ; *Tel:* +9821-22970052 ; *Fax:* +9821-22970052

1. Introduction

Driven by buoyancy force, natural convection heat transfer has been widely used in many engineering applications such as cooling, heating, ventilation, and air conditioning. Since common fluids have low conductive heat transfer, using high power and temperature systems and improving natural convection heat transfer are essential [1,2]. Therefore, some additives are used to improve these properties [3]. These additives can be metallic or non-metallic particles with higher conduction heat transfer than base fluids. When we add these particles to the fluids in small sizes, the thermal properties of the mixture improve [4]. After the publication of Maxwell's theory [5,6], many experimental and theoretical studies were published in this field. Maxwell showed that adding a certain volume fraction of particles to the fluids would increase the conduction heat transfer of the mixtures. On the other hand, other physical properties of the fluid, such as the viscosity, density, and heat capacity of the fluid, are affected, as well as thermal conductivity. Therefore, many studies have been conducted to evaluate the effects of these additives.

First, added particles were in millimeter and micron dimensions, but more attention should have been paid to these particles due to high corrosion and pressure drop as well as high sedimentation speed. Adding nanoparticles (1-100 nm) to the fluids solved these problems. Further, several studies have been carried out on the homogeneity of the nanoparticle distribution in the mixture. For example, Putra *et al.* studied copper oxide-water and aluminum oxide-water nanofluids at different volume fractions and observed that the nanofluids have a homogeneous behavior [7].

In computational fluid dynamics, nanofluids can be modeled as single- and two-phase flow. In the single-phase model, the nanofluid is considered fluid, and only one set of conversion equations is solved. In addition, the physical properties of the mixture, extracted from the experimental tests, are replaced with the physical properties of the pure fluid. Izadi *et al.* investigated the forced convection of a nanofluid inside an annulus [8]. They used a single-phase model to simulate the flow. In their study, velocity profiles were not affected by the volume fraction changes, while the temperature profiles were affected by the concentration of nanoparticles. In another study, Kaya investigated the turbulent flow of nanofluids inside a square channel using the single-phase model [9]. The results showed that heat transfer, pressure drop, and shear stress on the wall increased by increasing volume fraction and Reynolds number. Ziad Saghir *et al.* investigated the heat transfer of nanofluids flowing inside a cavity and showed that increasing the Rayleigh number and volume fraction of nanoparticles decreased heat transfer [10].

There have been several studies that focused on the natural convection heat transfer. Ternik *et al.* evaluated the natural convection of a non-Newtonian nanofluid inside a cavity [11]. They used non-Newtonian power law to model the viscosity of nanofluid. The results indicated an enhancement in heat transfer for different nanofluids. Maliki *et al.* [12] and Mehryan *et al.* [13] studied the natural convection heat transfer inside a cavity. The cavity was exposed to a magnetic field, and the Boltzmann lattice method was used for simulation. The results demonstrated that the heat transfer rate increased with increasing Rayleigh and decreasing Hartmann numbers.

After studying natural convection flow in square cavities modeled by the single-phase method, Khanafer *et al.* concluded that increasing the volume fractions of nanoparticles in each Rayleigh number range increased the cavity's heat transfer rate [14]. Ho *et al.* experimentally investigated the square cavities of different sizes [15]. They observed that heat transfer could be improved only at low nanoparticle concentrations in the mixture and high Rayleigh numbers. The results would be reversed if these conditions were different, and consequently, the heat transfer rate would be diminished. Other empirical studies show a decrease in heat transfer in the cavities with these conditions [7,16-17]. Kamal Tiwari *et al.* numerically investigated a square cavity with vertically moving walls [18]. The results indicated that the rate of heat transfer completely depended on the direction and velocity of the walls, and with increasing volume fraction of nanoparticles, the Nusselt number increased nonlinearly.

The two-phase method is divided into Eulerian and Lagrangian categories. The mixture model, a subdivision of the Eulerian models, only solves one set of equations for each phase instead of solving one set of equations for the base fluid and a volume fraction equation for the second phase. Behzadmehr *et al.* modeled a nanofluid flow in a tube with uniform heat flux to compare two-phase and single-phase models [19]. The results indicated that the mixture model obtained more accurate results than the other models.

In addition, Akbari *et al.* investigated the mixed convection heat transfer of aluminum oxide-water nanofluid and concluded that the numerical results of the two-phase model were more accurate than the single-phase model [20]. Alsabery *et al.* numerically studied non-uniform nanofluids flow inside square cavities with blocks in their center and observed that the block dimensions influenced the amount of heat transfer [21]. Hazeri Mahmel *et al.* numerically modeled a cavity containing water-copper nanofluid using the OpenFOAM toolbox using a two-phase mixture method and a non-Newtonian model of the power law for predicting viscosity [22].

Further, Cheng numerically examined a non-Newtonian nanofluid's natural convection heat transfer about a vertical truncated cone in a porous medium [23]. He analyzed the

effects of Brownian motion, Thermophoresis force, and Lewis number on the Nusselt number and power law model index and showed that the Nusselt number increased by increasing the power law model index. Mohammadpourfard evaluated the thermal behavior of a non-Newtonian and magnetically driven fluid inside a vertical rectangular channel where the base fluid was electrically conductive, using a two-phase mixture model for different magnetic fields [24]. He found that electrical conductivity influenced nanofluid behavior and compared the Nusselt numbers and friction coefficients with the Newtonian fluid state.

In a comparative study conducted by Abolfazl Fattahi, the rectangular channel offers the best thermal behavior by impregnating the hot area on the absorbent plate, resulting in a Nusselt number at least 72% higher than other geometries for Re = 18,000 [25]. At the highest Reynolds number, the rectangular channel can reduce pressure by 5% compared to other geometries. Performance evaluation criteria for the rectangular channel are 14 and 9%, respectively, for a volume deduction of 1 and 2% more than the triangular channel, which has the lowest performance value.

Few studies have focused on nanoparticle sedimentation, and many events that may occur during particle sedimentation have yet to be extensively studied. Meng *et al.* studied the natural convection heat transfer and sedimentation of particles inside a cavity containing nanofluids using OpenFOAM solvers related to a two-phase mixture model and compared the results with the experimental results [26]. Furthermore, Baghsaz *et al.* investigated the sedimentation time of nanoparticles in a porous media at different Rayleigh numbers using OpenFOAM solvers [27]. The results indicated that with the increase in the Rayleigh number, the settling time and the Nusselt number also increased. Another study by Olabia *et al.* investigated the use of nanofluids in heat exchangers for different geometries and announced that nanofluids significantly improve heat efficiency numerically and experimentally [28]. Kaouther Ghachem *et al.* performed a computational analysis on the effect of adding a hybrid nanofluid in a cross-flow heat exchanger with rectangular wavy channels [29]. They concluded that with the appropriate selection of nanoparticle volume fraction and flow rate, the size of the heat exchanger can be adjusted, and adding nanoparticles at a speed of over 50 mm.s^{-1} has a significant effect. A review study with the aim of providing up-to-date results on the performance of natural displacement of nanofluids in different cavities under various thermal conditions for different nanofluids, cavity shapes, base fluids, nanoparticle concentration, thermal conditions, parameters control (cavity slope and aspect ratio, and magnetic field inclination), and enhancement techniques were performed [30]. Azzawi and Al-damook investigated the natural displacement in an isosceles triangular-shaped chamber heated from below and cooled from the sides filled with porous media [31]. It is found that the plumelike patterns for the isotherms occur at $Ra = 2.5 \times 10^3$, with two rotating large vortices breaking into multi-smaller vortices as the length of the heater is increased. Natural convection in this two-dimensional chamber is simulated using the finite volume method. Full closed-form solutions are provided by Turkyilmazoglu and Duraihem for the fluid flow impacted by a perpendicularly applied uniform magnetic field inside a pipe of the triangular cross-section [32]. The results showed that the governing equation of pressure gradient-induced flow under the external magnetic field is reduced to the Helmholtz partial differential equation with Dirichlet boundary conditions on the scaled sidelines of the equilateral triangle. The velocity solution is then derived in terms of elementary exponential functions involving the magnetic strength parameter, or the Hartmann number, controlling the retarding effect of the magnetic field on the velocity profiles. The Lorentz force effects are clarified on the two-variable velocity variations as well as on the centerline velocity, volumetric flow rate, and wall shears.

In the present study, the transient sedimentation of the nanoparticles of 0.64% aluminum oxide - water nanofluid in cavities with circular, square, and triangular cross sections was simulated using non-Newtonian Bingham plastic method and validated using, combining, and developing several available solvers in the OpenFOAM toolbox. Further, the effect of the sedimentation on the heat transfer rate was investigated at different Rayleigh numbers inside these cavities, where nanofluid is naturally circulating due to wall temperature differences.

2. Governing equations

The present study used the OpenFOAM® v6.0 toolbox to develop a suitable solver to investigate particle sedimentation and natural convection heat transfer in the desired geometry. Hence, the two solvers in this toolbox, namely buoyant BoussinesqPimpleFoam and drift FluxFoam, were combined. The mixture method was used to simulate the two-phase state. The equations in this solver include a set of conservation equations for the nanofluid and a volume fraction equation for the second phase. Due to the density difference from the first phase, sedimentation of the secondary phase is used as a relative velocity equation in the momentum equation. The equations are as follows:

Continuity equation:

$$\frac{\partial \rho_m}{\partial t} + \nabla . (\rho_m U_m) = 0 \quad (1)$$

Momentum equation:

$$\frac{\partial \rho_m U_m}{\partial t} + \nabla.(\rho_m U_m U_m) = -\nabla p_m + \nabla.\left[\tau_m + \tau_m^T - \sum \varphi_k \rho_k U_{km} U_{km}\right] + \rho_b g \quad (2)$$

Energy equation:

$$\frac{\partial T}{\partial t} + \nabla.(TU_m) = \nabla.\left(\frac{k_{eff}}{\rho_m C_{p_m}}\right) \quad (3)$$

The relative velocity of the initial phase (fluid) to the mixture:

$$U_{fm} = \frac{\varphi_s \rho_s}{\varphi_f \rho_f} U_{sm} \quad (4)$$

The relative velocity of the second phase (nanoparticles) to the mixture is also based on the Vesilind equation [33]:

$$U_{sm} = \frac{\rho_f}{\rho_m} U_0 \, 10^{-A\varphi_s} \quad (5)$$

where U_0 is the settling velocity and A is the settling coefficient.

The nanofluid density is obtained using the following relation:

$$\rho_m = (1-\varphi_s)\rho_f + \varphi_s \rho_s \quad (6)$$

Specific heat capacity of nanofluid:

$$\rho_m C_{p_m} = (1-\varphi_s)\rho_f C_{p_f} + \varphi_s \rho_s C_{p_s} \quad (7)$$

Thermal expansion coefficient:

$$\beta_m = \frac{(1-\varphi_s)\rho_f \beta_f + \varphi_s \rho_s \beta_s}{\rho_m} \quad (8)$$

In the Boussinesq approximation, when the density is multiplied by gravitational acceleration instead of the fluid or the nanofluid density, the following equation is used to calculate the density [34]:

$$\rho_b = \rho_m \, [1 - \beta (T - T_0)] \quad (9)$$

To calculate the nanofluid conductivity, the relation of Maiga *et al.* was used [35]:

$$k_{eff,Maiga} = k_f (4.97\,\varphi^2 + 2.7\varphi + 1) \quad (10)$$

The effective viscosity of the nanofluid was obtained using the following relation (Vradis & Hammad [36]):

$$\mu_{eff} = \frac{\tau_y}{\sqrt{\dot{\gamma}\,\dot{\gamma}} + 1e - (\frac{\tau_y}{\mu_p})} + \mu_p \quad (11)$$

The shear stress is expressed as follows:

$$\tau_y = A\,(10^{b\varphi_s} - 10^b) \quad (12)$$

where $\dot{Y}$ is the strain rate tensor, A is the strain tensor coefficient, b is the strain tensor power, and μ_p is the plastic viscosity in which μ_p can be obtained as follows:

$$\mu_p = C\,\mu_f \, 10^{d\varphi} - 1 \quad (13)$$

where C is the plastic viscosity coefficient, and d is the plastic viscosity power.

The following equation was utilized to calculate the strain rate $\sqrt{\dot{Y}\,\dot{Y}}$ (Daniel Brennan [37]):

$$\frac{1}{2}\left(\sqrt{\dot{\gamma}\,\dot{\gamma}}\right) = 2\left[\left(\frac{\partial u}{\partial x}\right)^2 + \left(\frac{\partial v}{\partial y}\right)^2\right] + \left(\frac{\partial v}{\partial x} + \frac{\partial u}{\partial y}\right)^2 \quad (14)$$

Rayleigh number, local Nusselt number, and average Nusselt number relations (Ternik *et al.* [38]) were used as follows:

$$Ra = g\,\beta_m\,\Delta T\,L^3/\vartheta\alpha \quad (15)$$

$$Nu(y) = \left(\frac{k_{eff}}{k_f}\right)\left(\frac{\partial T}{\partial n}\Big|_{n=0} \frac{L}{T_h - T_c}\right) \quad (16)$$

$$\overline{Nu} = \int_0^L Nu(y)\,dy/L \quad (17)$$

3. Problem description

The present study investigated the effects of cross-section shapes of three cavities during nanoparticle sedimentation on the natural convection heat transfer of Al_2O_3-water nanofluid. The cavities had square, circular, and triangular cross-sections with the same hydraulic diameter (Fig. 1). Water and aluminum thermophysical properties are listed in Table 1. The thermal insulation of the cavities' horizontal sides and the vertical sides' constant temperature with each side's temperature difference, proportional to the Rayleigh number,

Table 1. Thermophysical properties of the nanofluid.

Nanofluid	Viscosity ($kg.m^{-1}.s^{-1}$)	Thermal conductivity ($W.m^{-1}.K^{-1}$)	Density ($kg.m^{-3}$)	Specific heat ($J.kg^{-1}.K^{-1}$)	Thermal expansion (K^{-1})
Water	8.87e-4	0.58	997	4179	2.7e-4
Al_2O_3		46	3600	765	6.3e-6

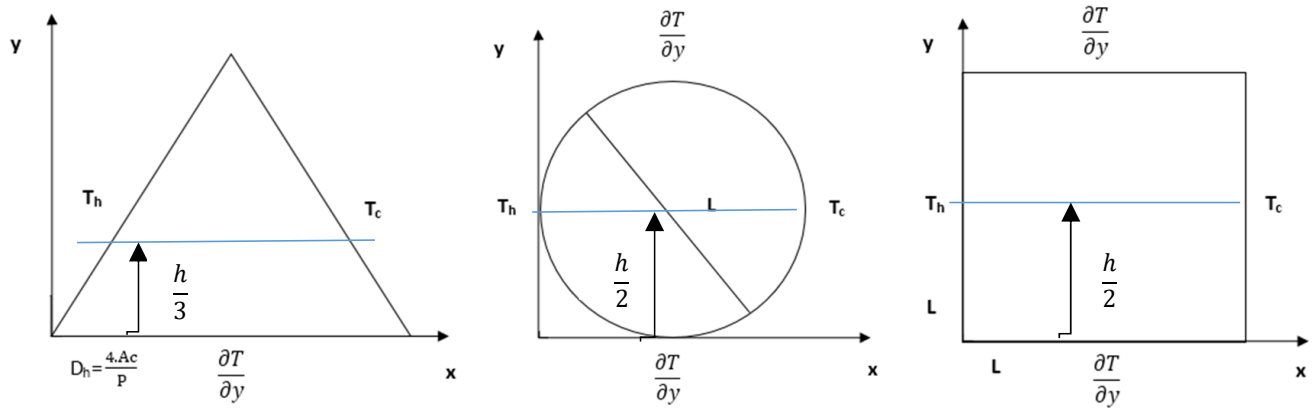

Fig. 1. Cross-sectional dimensions and boundary conditions.

were used as boundary conditions. The no-slip condition was applied to all surfaces, and the pressure gradient was zero for all the walls. The range of Rayleigh numbers for the present study was obtained from previous studies [14,38]. The problem was solved transiently to evaluate the sedimentation process over time. The volume fraction of nanoparticles was considered to be 0.64%.

4. Numerical procedure and developed solver validatio

The developed solver in the present study was obtained by combining two existing solvers from the OpenFOAM® v 6.0 toolbox, namely BuoyantBoussinesqPimpleFoam and driftFluxFoam. These solvers were used to model the heat transfer and settling, respectively, and these two phenomena were simulated in fluid flow by combining the two solvers. The PIMPLE algorithm was used to discrete the equations in the solver, combining two SIMPLE and PIZO algorithms in the finite volume method. The time steps were adjusted to the Courant number, whose maximum and minimum values were calculated to be 5 and 1, respectively. Gauss linear, Gauss linear corrected, and Gauss linear were used to obtain the gradient, Laplacian, and divergence parameters, respectively, according to Meng *et al.* [26]. The main process is given in a simplified flow chart shown in Fig. 2.

Since our approach in this project is a mixed method, we selected the only solver in the multiphase flows folder that uses this method, the driftFluxFoam. As previously stated, this solver has no energy equation and includes volume fraction, continuity, and momentum equations. There are different solvers in the heat transfer folder, but our preferred solver, which has both the energy equation and uses the Boussinesq approximation to simulate free movement, is buoyantBoussinesqPimpleFoam. We based our numerical work on the driftFluxFoam solver and added the rest of the needed items. i.e., we added the energy equation to the base solver folder and then added the energy equation after the speed equation in the main file of this solver, called C.driftFluxFoam. The speed value was initially obtained from the continuity and momentum equations. Then, this value was placed in the energy equation, and the temperature in different cells (which is the only unknown in the equation) was calculated. This file is the cornerstone of this solver, and all the steps that will be taken to solve a problem are coded in

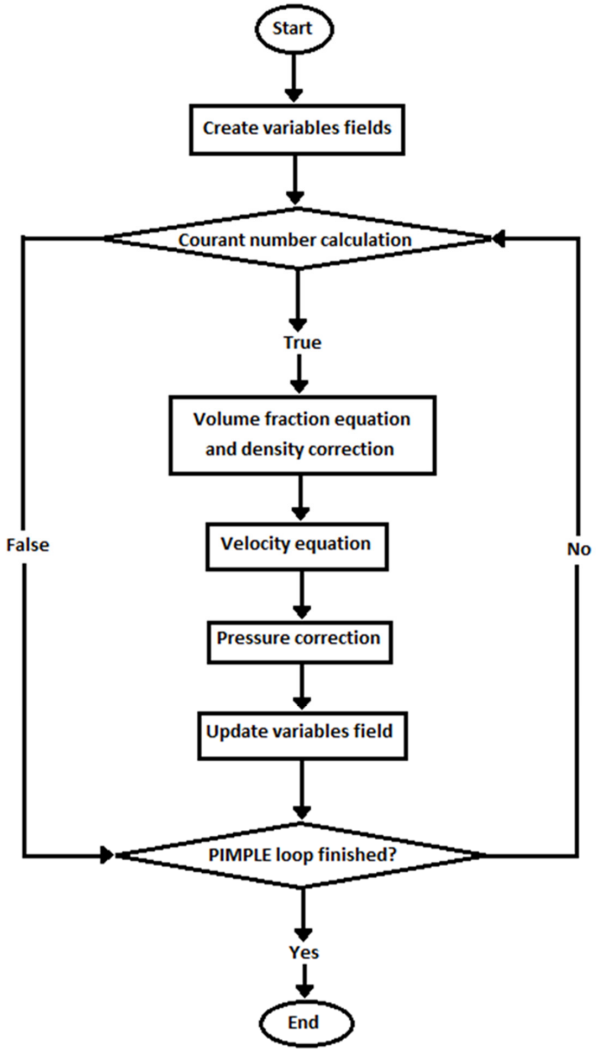

Fig. 2. The flow chart of solver 'driftFluxFoam'.

this file. We called the new solver boussinesqDriftFluxFoam, which is a combination of a thermal model with an approximation of Boussinesq and a mixed multiphase model, and replaced this name with driftFluxFoam in all required files. We added all the new parameters in the H.createFields file, and as one of the important points, every parameter that is based on one of the properties of speed, volume fraction, or temperature is added at the end of the equation file, which is the H.Ueqn. In addition, H. alphaEqnSubCycle and H.TEqn were added to update each time the problem is solved in different time steps, and the new value is placed in the next cycle. Finally, we went to the momentum equation, entered the equations in this file, and defined the parameters related to thermophoresis and Brownian diffusion. For example, we copy one of the examples in the Tutorials folder that uses the driftFluxFoam solver to the run folder. The geometry was easily entered in the blockMesh file, and the linear Gauss, corrected linear Gauss, and linear Gauss schemes were used for the gradient, elpalsine, and divergence of the parameters, respectively.

Different mesh sizes were examined, and an optimum mesh was obtained for more accurate results. Several uniform grids with 40×40, 50×50, 60×60, 70×70, 80×80, 90×90, and 100×100 were tested, and the results showed that the grid generated with 80×80 cells was suitable (Table 2). A type of structured mesh was used for all three types of sections. As shown in Fig. 3, the temperature diagram along the horizontal line in the middle of the square cavity is confirmed by comparing the results with the numerical results of Khanafer *et al.* [14].

After validating the temperature of the solver without the effects of the two-phase relative velocity, nanoparticle sedimentation time was compared with the experimental results of Wen *et al.* [39] and numerical results of Meng e*t al.* [26] (Figs. 4-6).

Finally, the results proved that the developed solver can model heat transfer and sedimentation. Square, circular, and triangular cavities were modeled with the same hydraulic

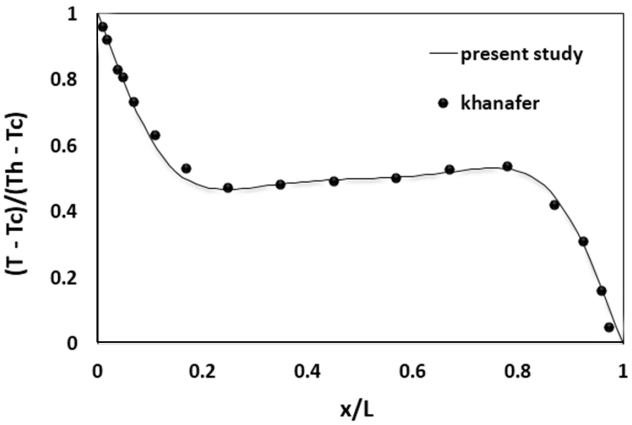

Fig. 3. 10% Copper-water nanofluid temperature validation along the horizontal line in the middle of the square cavity at Rayleigh 6.2×10^4 compared with the results of Khanafer *et al.* [14].

diameter, and as in the previous case, a uniform mesh was generated on them. As shown in Fig. 7, the mesh is sufficiently dense near the wall to enhance the simulation accuracy. The fluid inside the cavity was initially static, and the nanoparticles were homogeneously distributed within the fluid with a volume fraction of 0.64%. Two constant temperatures and two insulation boundary conditions were applied for all three geometries. The cooler wall temperature was constant, while the other varied from 302 to 320 K, depending on the Rayleigh number. The settings for all simulations were the same as the validation mode.

Fig. 8 displays the variations of the average Nusselt number of high-temperature walls over time for different geometries at $Ra = 10^5$. In all cases, the Nusselt number initially decreased with a steep slope until it finally reached a minimum value. The time to reach the minimum value of the Nusselt number was different for different geometries. The Nusselt number of the triangular cross-section reached its minimum value quicker than the other geometries, whereas its magnitude was more than the other geometries. The Nusselt number increased from a minimum to a constant value. The time duration of the simulation was 300 minutes, and during this interval, the

Table 2. Average Nusselt number for different grid numbers of sample in a steady state condition at Rayleigh 10^5.

Grid numbers Circular sample	40×40	50×50	60×60	70×70	80×80	90×90	100×100
$\overline{Nu}$	1.85	1.96	2.05	2.23	2.27	2.27	2.28
Grid numbers Square sample	40×40	50×50	60×60	70×70	80×80	90×90	100×100
$\overline{Nu}$	1.78	1.85	1.89	1.94	2.02	2.03	2.04
Grid numbers Triangle sample	40×40×40	50×50×50	60×60×60	70×70×70	80×80×80	90×90×90	100×100×100
$\overline{Nu}$	1.90	1.01	2.12	2.21	2.22	2.22	2.23

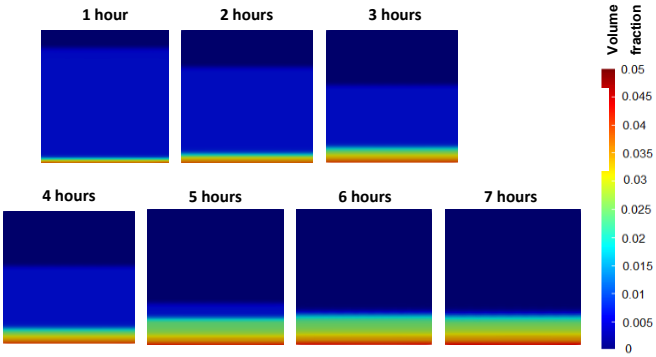

Fig. 4. Transient modeling of 0.64% Aluminum oxide-water nanofluid sedimentation inside a 2-dimensional cavity obtained by driftFluxFoam solver.

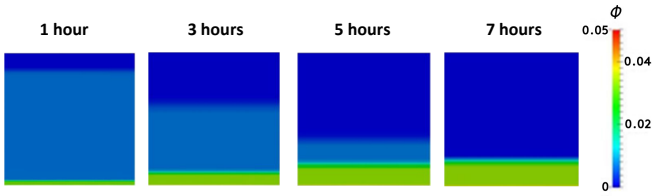

Fig. 5. Transient modeling of 0.64% Aluminum oxide-water nanofluid sedimentation inside a 2-dimensional cavity obtained by driftFluxFoam solver (Meng *et al.* [26]).

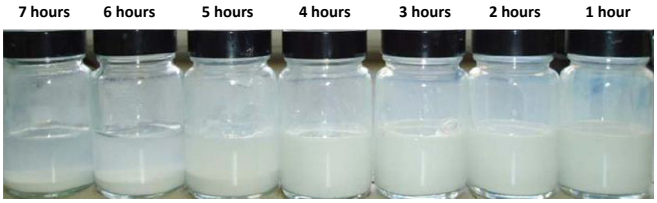

Fig. 6. The changes in 0.64% Aluminum oxide-water nanofluids (without any stabilizer) stability over time (Wen *et al.* [39]).

circle and triangle Nusselt values were approximately 2.20, while the Nusselt number corresponding to the square cross-section was 1.86, about 15 less than the other geometries.

In order to more accurately examine the Nusselt variations of the three different geometries, the velocity vectors and volume fraction distribution of the nanoparticles were obtained at 10, 50, and 300 minutes (Fig. 9). By transferring heat to the fluid adjacent to the high-temperature wall, the fluid was heated, its density decreased, and thus the fluid moved upward. Viscosity and density are two important factors in free convection. Adding nanoparticles to the fluid increases the nanofluid's density and effective viscosity. Therefore, there will be a non-uniform distribution of the nanoparticles, viscosity, and density of the nanofluid at the beginning of the sedimentation process. As shown in Fig. 8, the settling is yet to be dominant in the cavity at 10 minutes, so free convection circulates throughout the cavity, and due to its high viscosity and effective density, the velocity of free convection and, consequently, the Nusselt number is low.

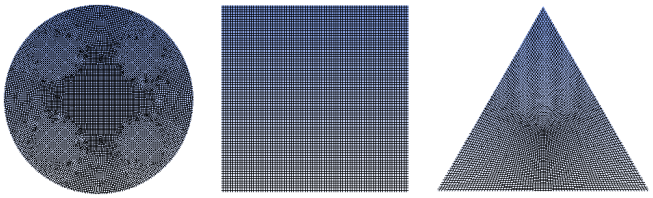

Fig. 7. Mesh of the three cavities. Structured mesh has been used for all three sections. For meshing, each side of the square and triangle is divided into 80 parts, and for the circle, the meshing is done so that the number of cells and nodes for all three sections is close to each other.

circle and triangle Nusselt values were approximately 2.20, while the Nusselt number corresponding to the square cross-section was 1.86, about 15 less than the other geometries.

In order to more accurately examine the Nusselt variations of the three different geometries, the velocity vectors and volume fraction distribution of the nanoparticles were obtained at 10, 50, and 300 minutes (Fig. 9). By transferring heat to the fluid adjacent to the high-temperature wall, the fluid was heated, its density decreased, and thus the fluid moved upward. Viscosity and density are two important factors in free convection. Adding nanoparticles to the fluid increases the nanofluid's density and effective viscosity. Therefore, there will be a non-uniform distribution of the nanoparticles, viscosity, and density of the nanofluid at the beginning of the sedimentation process. As shown in Fig. 8, the settling is yet to be dominant in the cavity at 10 minutes, so free convection circulates throughout the cavity, and due to its high viscosity and effective density, the velocity of free convection and, consequently, the Nusselt number is low.

Due to the proximity of high and low temperatures and the presence of a high-temperature gradient at the upper vertex of the triangular cross-section, a secondary flow was formed near the upper vertex, causing a higher average Nusselt number at the initial moments in comparison with the other two geometries. Over time and with the beginning of the sedimentation process, the volume fraction of the nanoparticles decreased at the upper side of the geometry and increased at the lower side. Accordingly, the free

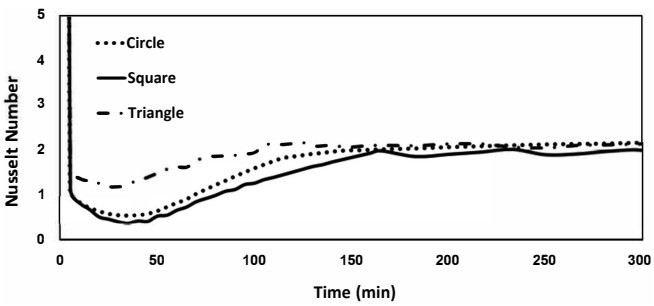

Fig. 8. Variations of Nusselt number in different geometries over time at Rayleigh = 10^5.

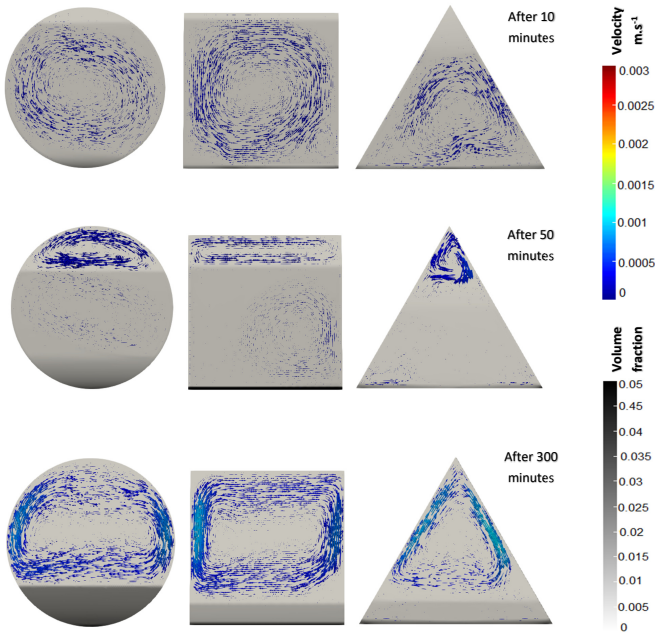

Fig. 9. Velocity vectors at different moments (Ra=10^5).

convection flow was formed in the dilute part of the mixture, in which the dimensions and power of the flow increased over time, and consequently, the volume of the primary flow decreased. This process continued until the sediment layer reached its final value, and due to the high volume fraction of the nanoparticles in the lower part of the section, the purified fluid was approximately static, and the volume of the diluted fluid reached a constant value, which did not change over time, indicating that the process reached a steady state condition.

It can be seen from Figs. 10 and 11 that as the Rayleigh number increases, the Nusselt number increases independent of the geometry of the cavities. The sedimentation time is a function of the Rayleigh number such that the investigated cavities hydrodynamically and thermally converged at Rayleigh 10^5 after about 200 minutes, at Rayleigh number 5×10^5 after 250 minutes, and at Rayleigh number 10^6 after 300 minutes.

The histogram of the Rayleigh numbers versus Nusselt numbers for different cross-sectional shapes of the cavity is presented in Fig. 12 to more accurately compare the results of the models in the steady state condition. This figure demonstrates that the Nusselt number increases for all geometries by increasing the Rayleigh number. In the small Rayleigh numbers, the Nusselt number is approximately equal for all three geometries, while by increasing these amounts, the Nusselt number in the square cavity grows more than others due to more space of cavity to fluid flow. Finally, in a high Rayleigh number, the triangular cross-section is less thermally efficient than the square and circular ones, and the square cavity has the highest heat transfer.

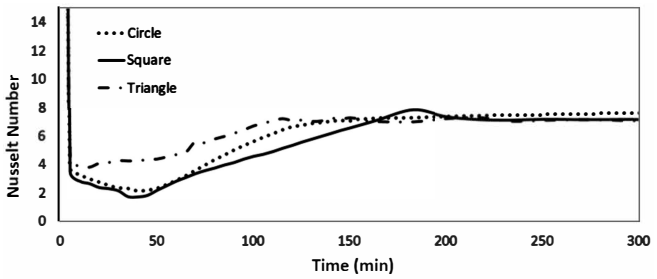

Fig. 10. Nusselt number values during transient sedimentation of nanoparticles in three cavities with different cross-sectional shapes and 5×10^5 Rayleigh number.

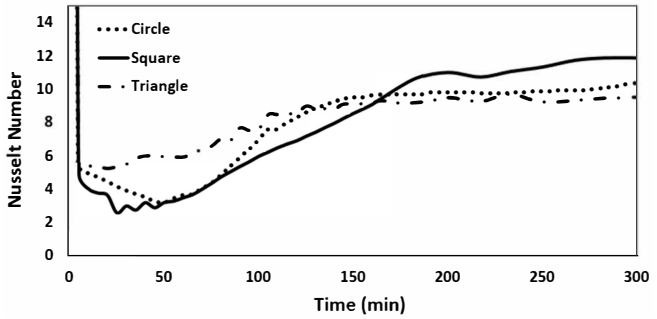

Fig. 11. Nusselt number values during transient sedimentation of nanoparticles in three cavities with different cross-sectional shapes and 10^6 Rayleigh number.

Fig. 13 is presented to better visualize the fluid flow during the sedimentation process in different cross-sections. As shown in Fig. 13, two circulating flows exist in the cavities: one in the purified fluid part, which has a significant effect on increasing the Nusselt number, and the other occurs in the mixture part, which has a slower velocity due to higher viscosity. After completing the sedimentation process in the settled layer, with a high concentration of nanoparticles, there was no free convection, and the purified fluid flowed in the upper part of the cavity at a higher speed. The higher flow speed led to faster fluid homogenization, enhancing the Nusselt number. The space created in the square cavity for purified fluid was wider than the space created in the circle and triangle cross-section, and this caused more heat absorption by the fluid. Thus, the fluid temperature near the

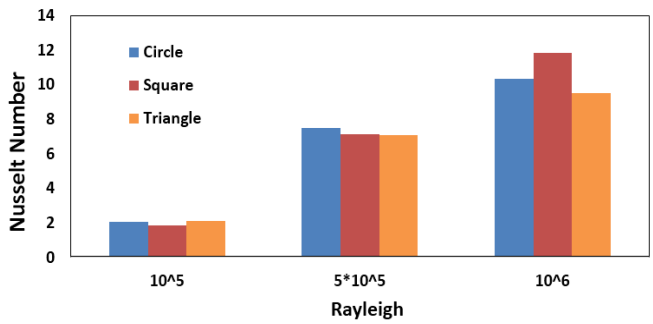

Fig. 12. Comparison of Nusselt numbers at different cross-sections and Rayleigh numbers in steady state condition.

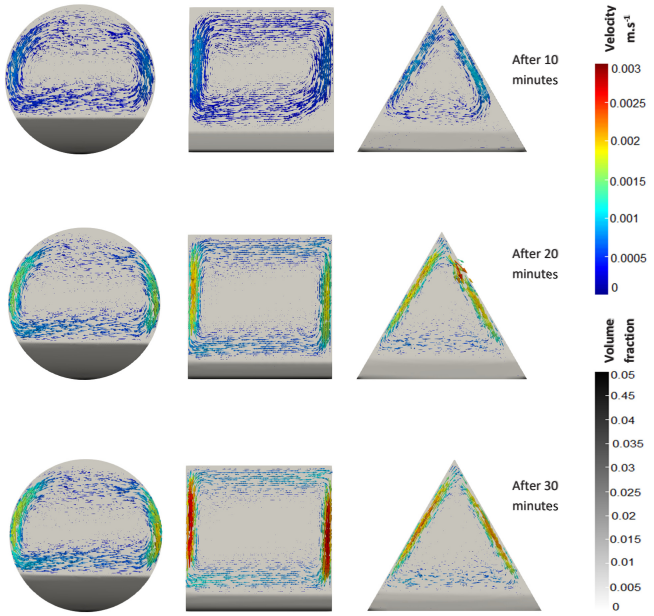

Fig. 13. From top to bottom, velocity vectors in steady state condition at Rayleigh numbers of 10^5, 5×10^5, and 10^6.

wall decreased with the heat dissipating toward the center of the cavity, providing conditions for the enhancement of the Nusselt number. In addition, the velocity of the circulating fluid in the square cavity and the upper Rayleigh numbers increased more than in the two other cavities, resulting in a faster homogeneity of the fluid temperature and enhancing the Nusselt number. The higher height of the settling layer in the circular cavity lessened the fluid circulation space and subsequently decreased fluid velocity. The contribution of the convective heat transfer decreased in the settling layer over the completion of the sedimentation, and the conduction heat transfer increased, reducing the total amount of heat transfer. Figs. 14-16 present a more accurate evaluation of the free convection flow velocity in the cavities.

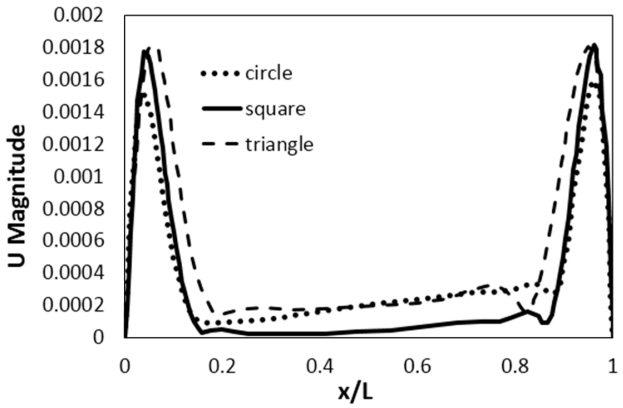

Fig. 15. Comparison of nanofluid velocity with Rayleigh number of 5×10^5 along the horizontal streamline passing through the centroid of the cavities.

At the center of the enclosures, velocity was very low, and the maximum velocity occurred near the wall. However, the minimum velocity in the circular cavity was higher than the others due to the higher sediment layer, while its maximum was lower than that of the square and the triangle. In low Rayleigh numbers, the free convection flow velocity in the triangle cavity was approximately the same as the square. However, by increasing the Rayleigh number, the velocity in the square cavity increased significantly. Although it was lower in the minimum points, there was good circulation in this cavity, leading to a higher Nusselt number. In the sedimentation layer of the triangle, the two sharp angular edges trapped a high volume fraction of nanoparticles, which caused more variations of the Nusselt numbers in this case. However, this trapping did not occur at the two upper corners of the square. In the upper Rayleigh numbers, the settling layer moved in the same direction as the purified fluid flow due to friction, and obviously, the nanoparticles were more concentration toward the end of this direction.

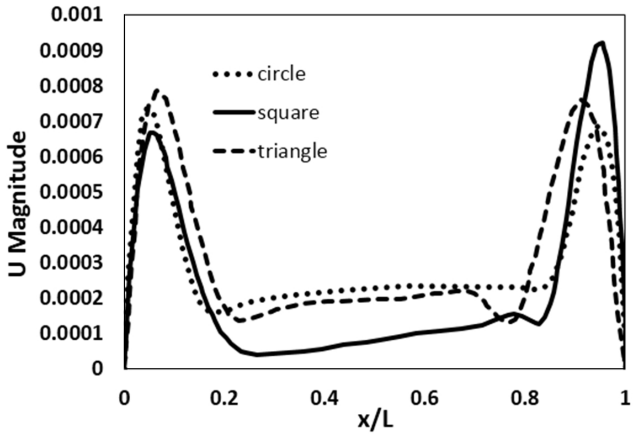

Fig. 14. Comparison of nanofluid velocity with Rayleigh number of 10^5 along the horizontal streamline passing through the centroid of the cavities.

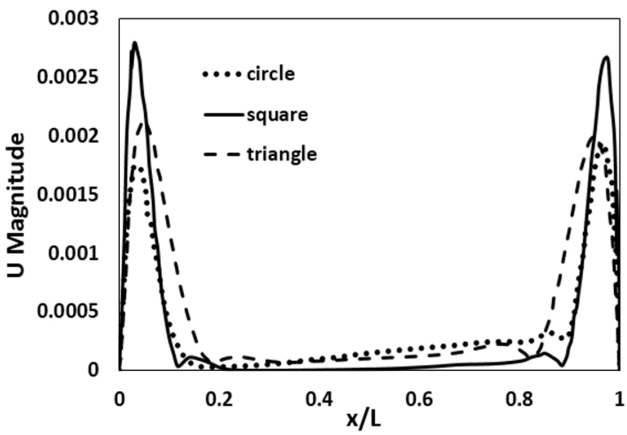

Fig. 15. Comparison of nanofluid velocity with Rayleigh number of 10^6 along the horizontal streamline passing through the centroid of the cavities.

Regarding sedimentation process time, the triangular and square cross-sections had the earliest and longest time, respectively. Although this time was not very significant, one of the reasons for earlier sedimentation at a triangular cross-section, in addition to its geometry, was the nanoparticles' high volume fraction stored at the corners since there would be more space at the center of the lower side of the cavity while the settling in square enclosure occurred uniformly.

3. Conclusion

A new solver in an open-source framework, Open Foam, was developed to study the thermal behavior of the Al_2O_3-water nanofluid in three different cross-sections, including square, triangular, and circular. The results showed that in the absence of any stabilizer, the nanoparticle sedimentation significantly affects the nanofluid's thermal behavior. The cross-section geometry of the enclosure and the Rayleigh number are two significant parameters influencing the settling time and the Nusselt number. The comparative study revealed that the square cavity has the highest Nusselt number, which could be improved by increasing the Rayleigh number. There is no significant difference between the settling times of different geometries due to the completely uniform settling of the nanoparticles in the square cavity and the non-uniform settling in circular and triangular ones; the triangular and square cross sections have the shortest and longest sedimentation time, respectively. Further, the results indicated that in the triangle sedimentation layer, a significant volume fraction of the nanoparticles was trapped at the two lower corners of a triangle, which caused faster sedimentation and a fluctuation in the other obtained data.

Disclosure statement

No potential conflict of interest was reported by the authors.

References

[1] Kefayati. GH. R. (2016). Simulation of Double Diffusive Natural Convection and Entropy Generation of Power-Law Fluids in An Inclined Porous Cavity with Soret and Dufour Effects (Part II: Entropy Generation). *International Journal of Heat and Mass Transfer*, *94*, 582-624. https://doi.org/10.1016/j.ijheatmasstransfer.2015.11.043

[2] Das. D., Roy. M., & Basak. T. (2017). Studies on Natural Convection within Enclosures of Various (Non-square) Shapes – A Review. *International Journal of Heat and Mass Transfer*, *106*, 356-406. https://doi.org/10.1016/j.ijheatmasstransfer.2016.08.034

[3] Liu. K. V., Choi U. S., & Kasza K. E. (1988). *Measurements of Pressure Drop and Heat Transfer in Turbulent Pipe Flows of Particulate Slurries*. NASA STI/Recon Technical Report, Argonne National Laboratory, ANL-88-15. https://digital.library.unt.edu/ark:/67531/metadc282865/m2/1/high_res_d/metadc282865.pdf

[4] Nalwa H. S. (2004). *Encyclopedia of Nanoscience and Nanotechnology*, Vol. 6, pp. 757-759.

[5] Maxwell J. C. (1873). *Electricity and Magnetism,* Clarendon Press, Oxford.

[6] Maxwell J. C. (1904). *A Treatise on Electricity and Magnetism*, Oxford University Press, Cambridge.

[7] Putra, N., Roetzel, W. & Das, S.K. (2003). Natural Convection of Nano-Fluids. *Heat and Mass Transfer*, *39*, 775–784. https://doi.org/10.1007/s00231-002-0382-z

[8] Izadi. M., Behzadmehr. A., & Jalali-Vahida. D. (2009). Numerical Study of Developing Laminar Forced Convection of A Nanofluid in An Annulus. *International Journal of Thermal Sciences*, *48*, 2119-2129. https://doi.org/10.1016/j.ijthermalsci.2009.04.003

[9] Kaya. O. (2015). Numerical Investigation of Heat Transfer, Pressure Drop and Wall Shear Stress Characteristics of Al_2O_3-Water Nanofluid in a Square Duct. *Arabian Journal for Science and Engineering*, 40, 3641-3655. https://doi.org/10.1007/s13369-015-1790-y

[10] Ziad Saghir. M., Ahadi. A., Yousefi. T., & Farahbakhsh. B. (2016). Two-Phase and Single Phase Models of Flow of Nanofluid in A Square Cavity: Comparison with Experimental Results. *International Journal of Thermal Sciences*, *100*, 372-380. https://doi.org/10.1016/j.ijthermalsci.2015.10.005

[11] Ternik. P., & Rudolf. R. (2013). Laminar Natural Convection of Non-Newtonian Nanofluids in A Square Enclosure with Differentially Heated Side Walls. *International Journal of Simulation Modelling, 12*, 5-16. https://doi.org/10.2507/IJSIMM12 (1)1.215

[12] Mliki, B, Abbassi, M. A., Omri, A. & Zeghmati, B. (2015). Augmentation of Natural Convective Heat Transfer in Linearly Heated Cavity by Utilizing Nanofluids in the Presence of Magnetic Field and Uniform Heat Generation/Absorption. *Powder Technology*, *284*, 312-325. https://doi.org/10.1016/j.powtec.2015.06.068

[13] Mehryan, S. A. M., Izadi, M., Chamkha, A. J., & Sheremet, M. A. (2018). Natural Convection and Entropy Generation of A Ferrofluid in A Square Enclosure under the Effect of A Horizontal Periodic Magnetic Field. *Journal of Molecular Liquids*, *263*, 510-525. https://doi.org/10.1016/j.molliq.2018.04.119

[14] Khanafer, Kh., Vafai, K. & Lightstone, M. (2003). Buoyancy-Driven Heat Transfer Enhancement in A Two-Dimensional Enclosure Utilizing Nanofluids. *International*

Journal of Heat and Mass Transfer, *46*, 3639-3653. https://doi.org/10.1016/S0017-9310(03)00156-X

[15] Ho, C. J. & Liu, W. K., Chang, Y. S. & Lin, C. C. (2010). Natural Convection Heat Transfer of Alumina-Water Nanofluid in Vertical Square Enclosures: An Experimental Study. *International Journal of Thermal Sciences*, *49*, 1345-1353. https://doi.org/10.1016/j.ijthermalsci.2010.02.013

[16] Li, C. H., & Peterson, G. P. (2010). Experimental Studies of Natural Convection Heat Transfer of Al_2O_3/DI Water Nanoparticle Suspensions (Nanofluids). *Advances in Mechanical Engineering*, *2*, 742739. https://doi.org/10.1155/2010/742739

[17] Agwu Nnanna, A. G. (2007). Experimental Model of Temperature-Driven Nanofluild. *Journal of Heat Transfer*, *129*(6), 697-704. https://doi.org/10.1115/1.2717239

[18] Tiwari, R. & Das, M. (2007). Heat Transfer Augmentation in A Two-Sided Lid-Driven Differentially Heated Square Cavity Utilizing Nanofluids. *International Journal of Heat and Mass Transfer*, *50*, 2002-2018. https://doi.org/10.1016/j.ijheatmasstransfer.2006.09.034

[19] Behzadmehr, A., Saffar-Avval, M. & Galanis, N. (2007). Prediction of Turbulent Forced Convection of A Nanofluid in A Tube with Uniform Heat Flux Using A Two Phase Approach. *International Journal of Heat and Fluid Flow*, *28*, 211-219. https://doi.org/10.1016/j.ijheatfluidflow.2006.04.006

[20] Akbari, M., Galanis, N. & Behzadmehr, A. (2011). Comparative Analysis of Single and Two-Phase Models for CFD Studies of Nanofluid Heat Transfer. *International Journal of Thermal Sciences*, *50*, 1343-1354. https://doi.org/10.1016/j.ijthermalsci.2011.03.008

[21] Alsabery, A., Tayebi, T., Chamkha, A. & Hashim, I., (2018). Effects of Non-Homogeneous Nanofluid Model on Natural Convection in a Square Cavity in the Presence of Conducting Solid Block and Corner Heater. *Energies*, *11*, 2507-2518. https://doi.org/10.3390/en11102507

[22] Hazeri-Mahmel. N., Shekari. Y., & Tayebi. A. (2018). Numerical Study of Mixed Convection Heat Transfer in A Cavity Filled with Non-Newtonian Nanofluids Utilizing Two-Phase Mixture Model. *Amirkabir Journal of Mechanical Engineering*, *50*(6), 389-392. https://doi.org/10.22060/mej.2017.12504.5355

[23] Cheng. C.-Y. (2012). Free Convection of Non-Newtonian Nanofluids About A Vertical Truncated Cone in A Porous Medium. *International Communications in Heat and Mass Transfer*, 39(9), 1348-1353. https://doi.org/10.1016/j.icheatmasstransfer.2012.08.004

[24] Mohammadpourfard. M. (2015). Numerical Study of Magnetic Fields Effects on the Electrical Conducting Non-Newtonian Ferrofluid Flow Through A Vertical Channel. *Modares Mechanical Engineering Journal*, *15*(1), 379-389. http://dorl.net/dor/20.1001.1.10275940.1394.15.1.38.4

[25] Fattahi, A. (2021). The Effect of Cross-Section Geometry on the Performance of A Solar Nanofluid Heater in A Parabolic Solar Receiver: A Comparison Study. *Journal of the Taiwan Institute of Chemical Engineers*, *124*, 17-28. https://doi.org/10.1016/j.jtice.2021.05.014

[26] Meng, X., Zhang, X., & Li, Q. (2016). Numerical Investigation of Nanofluid Natural Convection Coupling with Nanoparticles Sedimentation. *Applied Thermal Engineering*, *95*, 411- 420. https://doi.org/10.1016/j.applthermaleng.2015.10.086

[27] Baghsaz, S., Rezanejad, S., & Moghimi, M. (2019). Numerical Investigation of Transient Natural Convection and Entropy Generation Analysis in A Porous Cavity Filled with Nanofluid Considering Nanoparticles Sedimentation. *Journal of Molecular Liquids*, *279*, 327-341. https://doi.org/10.1016/j.molliq.2019.01.117

[28] A.G. Olabi, Wilberforce, T., Sayed, E. T., Elsaid, K., Atiqure Rahman, S. M., & Abdelkareem, M. A. (2021). Geometrical Effect Coupled with Nanofluid on Heat Transfer Enhancement in Heat Exchangers. *International Journal of Thermofluids*, *10*, 100072. https://doi.org/10.1016/j.ijft.2021.100072

[29] Ghachem, K., Aich, W., & Kolsi, L. (2021). Computational Analysis of Hybrid Nanofluid Enhanced Heat Transfer in Cross Flow Micro Heat Exchanger with Rectangular Wavy Channels. *Case Studies in Thermal Engineering,* 24, 100822. https://doi.org/10.1016/j.csite.2020.100822

[30] Giwa, S. O., Sharifpur, M., Murshed, S. M. S., & Meyer, J. P. (2023). Application of Nanofluids: Natural Convection in Cavities. in S. S. Sonawane & M. Sharifpur (Eds.), *Nanofluid Applications for Advanced Thermal Solutions* (pp. 117-149), Elsevier. https://doi.org/10.1016/B978-0-443-15239-9.00005-9

[31] Azzawi, I. D. J., & Al-damook, A. (2022). Multi-Objective Optimum Design of Porous Triangular Chamber Using RSM. I*nternational Communications in Heat and Mass Transfer*, *130*, 105774. https://doi.org/10.1016/j.icheatmasstransfer.2021.105774

[32] Turkyilmazoglu, M., & Duraihem, F. Z. (2023). Fully Developed Fow in A Long Triangular Channel under An Applied Magnetic Field. *Magnetism and Magnetic Materials*, *578*, 170803. https://doi.org/10.1016/j.jmmm.2023.170803

[33] Vesilind, P. A. (1968). Theoretical Considerations: Design of Prototype Thickeners from Batch Settling Tests. *Water Sewage Works*, *115*(7), 302-307.

[34] Boussinesq, V. J. (1903). Théorie Analytique De La Chaleur: Mise En Harmonie Avec La Thermodynamique

Et Avec La Théorie Mécanique De La Lumière, Gauthier-Villars.

[35] Maïga, S., Nguyen, C., Galanis, N., & Roy, G. (2004). Heat Transfer Behaviors of Nanofluid in A Uniformly Heated Tube. *Superlattices and Microstructures*, *35*, 543-557. https://doi.org/10.1016/j.spmi.2003.09.012

[36] Vradis. G. C., & Hammad. Kh. J. (1995). Heat Transfer in Flows of Non-Newtonian Bingham Fluids Through Axisymmetric Sudden Expansions and Contractions. *Numerical Heat Transfer, Part A: Applications*, *28*(3), 339-353. https://doi.org/10.1080/10407789508913749

[37] Brennan D. & University of London. (2001). *The Numerical Simulation of Two Phase Flows in Settling Tanks* (Dissertation). University of London.

[38] Ternik, P., & Rudolf, R. (2012). Heat Transfer Enhancement for Natural Convection Fow of Water Based nanofluids in A Square Enclosure. I*nternational Journal of Simulation Modelling*, *11*(1), 29-39. https://doi.org/10.2507/IJSIMM11(1)3.198

[39] Wen, D., Lin, G., Vafaei, S. & Zhang, K. (2009). Review of Nanofluids for Heat Transfer Applications. *Particuology*, *7*(2), 141-150. https://doi.org/10.1016/j.partic.2009.01.007

Additional information

Correspondence and requests for materials should be addressed to M. Mahdi.

HOW TO CITE THIS ARTICLE

Mahdi, M.; Noori, A.; Farrokh, A. (2023). Numerical investigation of the Effect of Nanoparticle Sedimentation on the Thermal Behavior of Cavities with Different Cross-sectional Shape*s*. *J. Part. Sci. Technol. 9(2) 73-84.*

DOI: 10.22104/JPST.2024.6586.1245
URL: https://jpst.irost.ir/article_1353.html